Chemical Engineering Journal 405 (2021) 126608

Contents lists available at ScienceDirect

Chemical Engineering Journal

journal homepage: www.elsevier.com/locate/cej

Fabrication of molecularly imprinted polymers with tunable adsorption capability based on solvent-responsive cross-linker

Yahan Cui[a], Zhongyu He[a], Yang Xu[b], Yu Su[a], Lan Ding[a,*], Yi Li[c]

[a] College of Chemistry, Jilin University, 2699 Qianjin Street, Changchun 130012, PR China
[b] College of Life Sciences, Jilin University, 2699 Qianjin Street, Changchun 130012, PR China
[c] State Key Laboratory of Inorganic Synthesis and Preparative Chemistry, College of Chemistry, Jilin University, 2699 Qianjin Street, Changchun 130012, PR China

HIGHLIGHTS

- Solvent-responsive molecularly imprinted polymers (S-MIPs) were developed.
- The adsorption behavior of S-MIPs was regulated by solvent composition.
- S-MIPs were successfully employed to solvent-regulated separation of BPA in human urine.

GRAPHICAL ABSTRACT

Molecularly imprinted materials with switchable adsorption capability based on solvent-responsive cross-linker.

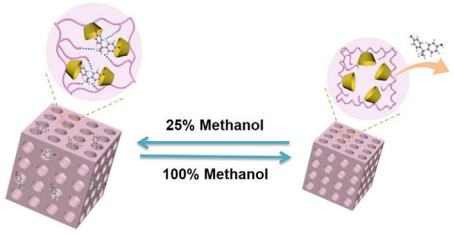

ARTICLE INFO

Keywords:
Stimuli-responsive polymers
Molecular imprinting
Solvent-responsiveness
Separation

ABSTRACT

The fabrication of facile and versatile adsorbents with switchable adsorption performance based on molecularly imprinting polymers is of great interest although still very challenging. Herein, a dynamic solvent-responsive poly (ethylene glycol) unit-containing chain was introduced as cross-linker to prepare solvent-responsive molecularly imprinted polymers (S-MIPs) by free radical polymerization. Acryloyl-modified beta-cyclodextrin was used as functional monomer, methacrylic acid as co-functional monomer and bisphenol A (BPA) as model template. BPA can be tightly adsorbed in recognition sites by host-guest interaction and hydrogen binding. Solvent-responsiveness of S-MIPs was investigated. Templates can be easily bound into the recognition cavity in 25% methanol aqueous solution with binding capacity of 21.36 mg/g while completely release in 100% methanol following the de-swelling of the imprinting cavity. Binding experiments demonstrated that S-MIPs displayed appreciable recognition capability and selectivity toward BPA in 25% methanol solution, well lining with Langmuir isothermal model and pseudo-second-order model. The proposed S-MIPs were successfully applied for the direct enrichment of BPA from human urine without protein pre-deposition process. Under the optimum conditions, the S-MIPs exhibited satisfactory recoveries ranging from 77.3% to 87.8% (spiked level from 40 μg/L to 800 μg/L), indicating excellent applicability for specific analytes removal from urine samples. This simple synthetic strategy provides an efficient route to synthesize the new intelligent materials for sample analysis in complicated biological matrixes.

1. Introduction

Molecularly imprinted polymers (MIPs) have attracted growing attention owing to their fascinating features of structure predictability and recognition specificity that endow them with universal applications including purification and separation [1–4], sensors [5–7], smart drug

* Corresponding author.
E-mail address: dinglan@jlu.edu.cn (L. Ding).

https://doi.org/10.1016/j.cej.2020.126608
Received 11 December 2019; Received in revised form 28 July 2020; Accepted 9 August 2020
Available online 12 August 2020
1385-8947/ © 2020 Elsevier B.V. All rights reserved.

delivery [8–10] and catalysis [11,12]. Particularly, development of MIPs for purification and separation has achieved great progress by emerging technologies. However, the application of MIPs in sample separation still encounters many challenges [13–15], such as partial template removal, low binding affinity, undesired selectivity and untunable identification performances. All drawbacks above remain to be addressed to meet the various requirements of actual analysis. Because of good responsiveness, switchable recognition characters and high binding capacity, stimuli-responsive MIPs (SR-MIPs) have been considered as one of the most potential candidates of absorbing materials [16–18]. These stimuli can be pH alternation [19–22], UV irradiation [23–25], temperature transformation [26–29], *etc*.. Although these existing SR-MIPs can effectively improve the absorption capacity and selectivity performances of MIPs to some extent, they still face some key problems that need to be solved in practical applications. For example, the utilization of pH-responsive MIPs always depends on the addition of a conventional acid or base. On the one hand, precise control of pH value of solution is of great importance for regulating the adsorption behavior of pH-responsive MIPs, but it is not easy to achieve. On the other hand, for template molecules that are sensitive to pH changes, higher or lower pH value would lead to their denaturation or even degradation, which will greatly limit the wide applications of these smart MIPs [30,31]. As for photo-responsive MIPs, although their employment could bring great advantages to sample preparation methodologies, the application of these functional materials in food and environmental analysis is relatively scarce. This can mainly ascribe to the fact: the rate of the photo-isomerization of photo-reactive monomer in highly cross-linked structure of MIPs is too low to meet the needs of rapid analysis, thus restricting their applications in environmental analysis [16]. Applications of SR-MIPs based on temperature-sensitive polymer for analytes separation must rely on the assistance of temperature controlling system, resulting in fussy experiments procedures and tremendous energy consumption [32]. Therefore, exploiting a facile and versatile type of SR-MIPs to meet the demands for actual analysis is highly desired.

In general, most MIPs were prepared in non-polar solvents upon H-bonding interactions between polymer and templates. When MIPs exposed to different organic solvents, corresponding shrinkage or swell of MIPs follows, deforming the selective binding sites thus further decreasing the recognition ability towards substrates [33]. Solvent plays a vital role in deciding the characters of binding and selectivity of MIPs. Therefore, making full use of solvent, will be of great importance to select the appropriate solvent for endowing the MIPs with excellent responsiveness performances and enhancing the separation efficacy. In the pioneering work, Mashelkar's group [34] has taken the application of MIPs as selective adsorbents for removal of phenol from BPA as example, aiming at elucidating the role of solvent for adsorption ability. In recent years, MIPs with solvent-responsiveness have been developed and reported. Maddalena et al. [35] has constructed molecular imprinted poly (acrylamide)-derivative nanogels with high selectivity to bind the target protein, showing their solvent-regulation capability upon the addition of acetonitrile. Liu's group have prepared a type of liquid crystalline-molecularly imprinted polymer, which displayed floating properties in water while immersed in acetonitrile, as floating drug delivery system to achieve controlled drug release [36]. Inspired by the above reports, we envision that a MIPs with solvent-responsiveness can be designed and synthesized so that one can make full use of the solvent difference between preparation process and sample analysis to achieve reversible adsorption/desorption for analytes.

In the proposed method, a dynamic cross-linker with solvent-responsiveness was firstly employed into the preparation of molecularly imprinted polymers. In order to further improve the adsorption property of the imprinting materials, beta-cyclodextrin derivative was used as functional monomer and methacrylic acid (MAA) was introduced to strengthen the selective sites. Taking advantages of their unique features, solvent-responsive molecularly imprinted polymers (S-MIPs) with high affinity for templates were obtained. The resultant S-MIPs combined the virtues of low-cost, easy of synthesis and high preparation yield. More importantly, the adsorption character of S-MIPs can be regulated just by adjusting the solvent composition. The template molecules could be hosted tightly in binding sites in 25% methanol aqueous solution while be eluted easily in 100% methanol. And S-MIPs possessed specific selectivity to target molecule comparing to its analogues. The prepared S-MIPs were directly utilized to solvent-regulated separation of BPA in human urine, indicating its great application potential in complicated samples.

2. Experimental section

2.1. Reagents

Bisphenol A (BPA), diphenolic acid (DPA), resorcin (RF), 2,2-azoisobutyronitrile (AIBN), methylacrylic acid (MAA), beta-cyclodextrin (β-CD), methacryloyl chloride (MA) were purchased from Liaoning Quanrui Reagent Co. Ltd (Jinzhou, China). Triethylene glycol dimethacrylate (TEGDMA), N, N-dimethylformamide (DMF), dimethyl sulfoxide (DMSO) and triethylamine were obtained from Aladdin Reagent Co. Ltd. (China). β-CD was recrystallized from water and dried under vacuum at 120 °C. All the other reagents in the present work were analytical grade without any purification. Deionized water used throughout the experiments was acquired by the laboratory purification system.

2.2. Instruments

Fourier transmission infrared spectra (FT-IR) were recorded on a Nicolet 360 spectrometer (Madison, USA). The morphologies of the relevant absorbents were observed by scanning electron microscope (SEM, Hitachi SU8000, Tokyo, Japan). Thermo gravimetric analysis (TGA) was carried out by using a TGA Q500 Thermal Analyzer Instrument (TA, USA). UV–Vis adsorption spectra were recorded by a Shimadzu UV-2550 spectrophotometer (Shimadzu, Japan).

Chromatographic analysis was performed on an Agilent 1100 liquid chromatograph (Palo Alto, CA, USA) which was equipped with a quaternary pump, a heated column compartment, a diode array detector (DAD) and a LC workstation. The detection wavelength was 224 nm for BPA. The mobile phase was methanol–water solution (60/40, v/v). The flow rate was 0.5 mL/min. The injection volume was set as 10 μL and the column temperature was 30 °C. An Agilent ZORBAX SB-C18 column (250 mm × 4.6 mm, 5 μm, Aglient, USA) was used throughout.

2.3. Preparation of solvent-responsive MIPs (S-MIPs)

2.3.1. Synthesis of vinyl modified β-CD (β-CD-MA)

β-CD-MA was obtained through the acylation reaction of β-CD with MA. Amount of β-CD (0.5 g) was placed to a 100 mL round-bottomed flask containing dry DMF (10 mL) and completely dissolved by ultrasonication. Then, 2.5 mL of dry triethylamine was injected to the above mixture at once in an ice bath. MA (1.25 mL) was dropwise injected into the above mixtures using a syringe under N_2 protection. After injection, the temperature was slowly elevated to 30 °C. The reaction system was stirred for another 0.5 h, followed by filtration to remove the unreacted β-CD. Then excess acetone was poured into the yellowish filtrate to obtain white precipitates. The precipitates were then collected by centrifugation, recrystallized twice with acetone, and dried at 50 °C for 24 h. The final white powder was denoted as β-CD-MA.

2.3.2. Synthesis of BPA-imprinted solvent-responsive polymers (S-MIPs)

The as-synthesized β-CD-MA (2 mmol, 100 mg) and BPA (1 mmol, 10 mg) were firstly dissolved in 1.5 mL DMSO. Then, MAA (3 mmol, 4 mL) was dropwise injected to the solution. The above mixture was pre-assembled by ultra-sonication at room temperature for 1 h.

Subsequently, 60 mmol of TEGDMA was poured into the above system, which was degassed for another 30 min in an ultrasonic bath. Afterwards, the mixture was transferred to a 100 mL round-bottomed flask with continuously stirred for 10 min, which was slowly filled with N_2. Then, 0.12 mmol AIBN was added to the flask, which was maintained under slightly stirring for 5 h and kept stand for another 19 h at 60 ˚C. After the polymerization reaction was completely finished, the crude mixture exhibited colorless transparent hydrogel. Furthermore, the crude hydrogel was washed with methanol-acetic acid mixture (9:1, v:v) for 24 h in Soxhlet extractor until no BPA could be detected. Then, the crude hydrogel was washed twice with methanol. Finally, the prepared S-MIP was dried in a vacuum at 50 ˚C for 24 h. The non-imprinted polymers (S-NIPs) were synthesized using the same routes described above except that no BPA molecules were added.

2.4. Adsorption experiments

Static adsorption experiments were conducted in 4 mL plastic pipe. A 10 mg amount of MIPs was dispersed in a series of 3 mL BPA aqueous solutions with various initial concentrations (C_o, mg/L) ranging from 5 to 100 mg/L. After the above mixture were mechanically shaken with 200 rpm/min for 24 h at room temperature, the S-MIP or S-NIP nanoparticles were separated *via* centrifugation. Then the equilibrium concentration of BPA (C_e, mg/L) in the supernatant was measured by UV–vis spectrophotometer operating at 278 nm. The binding amount of BPA on S-MIPs or S-NIPs at equilibrium, termed as the equilibrium adsorption capacity (Q_e, mg/g), could be calculated using the below Eq. (1):

$$Qe = \frac{Co - Ce}{m} V \quad (1)$$

where V (L) represents the volume of BPA solution and m (g) denotes the mass of MIPs or NIPs used.

The binding kinetics experiments were also carried out following a similar procedure with the static adsorption study to confirm the minimum adsorption equilibrium time. MIPs or NIPs (10 mg) were suspended to 3 mL of BPA solution with an initial concentration (C_o) of 50 mg/L. The obtained suspension was shaken continuously for a series of time internals from 5 min to 150 min at room temperature. The real-time concentration of BPA (C_t, mg/L) in the supernatants was monitored by UV–vis spectrometer. The binding amounts for BPA with different determined time t, defined as the temporal adsorption capacity (Q_t, mg/g), was calculated as Eq. (2):

$$Qt = \frac{Co - Ct}{m} V \quad (2)$$

The selectivity tests were evaluated towards 50 mg/L of BPA, DPA and RF in 25% methanol aqueous solution, respectively. The operating conditions were consistent with the static adsorption tests. After centrifugation, the supernatants of three substances were measured by UV–vis spectroscopy at 278 nm, 274 nm and 273 nm for BPA, DPA and RF, respectively. The selectivity of the S-MIPs was evaluated by the selectivity factor (α) that was calculated by the following Eq. (3):

$$\alpha = Q_{tem}/Q_{ana} \quad (3)$$

where Q_{tem} and Q_{ana} (mg/g) are the amount of templates and analogues adsorbed by S-MIPs, respectively.

2.5. Solvent-regulated uptake and release studies

The extended solvent-regulated studies were carried out under the alternately solvent switches. Briefly, 10.0 mg of S-MIPs in 3 mL of mixture solution was used. The initial concentration of BPA was pre-set at 50 mg/L. The solvent composition was firstly arranged with 25% methanol aqueous solution overnight and next transferred to 100% methanol, respectively. The above process was repeated three times. At the end of each cycle, the mixture system was centrifuged, and the residual supernatant was measured by UV–vis detector at 278 nm.

2.6. Determination of BPA in human urine

The human urine samples were obtained from a healthy volunteer. The urine samples were centrifuged at 8000 rpm for 8 min and the supernatant was filtered with an aqueous filtration membrane (0.45 μm pore size) for subsequent solid phase extraction.

An amount of 70 mg S-MIPs was put into a 10 mL centrifugal tube and conditioned with 3.0 mL 25% methanol aqueous mixture. Then the S-MIPs were separated by centrifugation and the supernatant was discarded. The conditioned S-MIPs and 5 mL of the urine samples were added into a beaker. The mixture was stirred for 30 min. After the extraction was completed, the S-MIPs were separated by centrifugation and washed with ultrapure water (0.5 mL). The analytes were obtained from the S-MIPs by methanol (4 × 1 mL) with the aid of ultrasound (for 2 min during each eluting process). Finally, the eluent was merged and dried with rotary evaporation. The residues were reconstituted with methanol (1 mL), filtered through a 0.45 μm membrane, and further analyzed by HPLC-DAD at 224 nm.

3. Results and discussion

3.1. Preparation of the S-MIPs

Herein, we put forward a new and simple route to construct S-MIPs where flexible poly (ethylene glycol) unit-containing chain as solvent-responsive cross-linker while functional monomer β-CD-MA is mainly responsive for the selective recognition sites. Besides, co-functional monomer of MAA was utilized to strengthen the binding interaction by forming the strong hydrogen interaction with hydroxyl group of BPA. The preparation process of S-MIPs and its possible recognition mechanism for templates are schematically illustrated in Fig. 1a**.** In detail, β-CD-MA with vinyl groups was firstly prepared through the acylation reaction of β-CD with MA. Then β-CD-MA, MAA and templates formed a pre-assembly complex by host-guest interaction and hydrogen bonding interaction. The incorporation of TEGDMA not only increased hydrophilicity of polymeric network but also endowed the imprinting materials with solvent-responsiveness [37]. The as-synthesized S-MIPs adsorbed the targeted molecules in 25% methanol aqueous solution, while released target molecules in 100% methanol due to the destruction of host-guest interaction between templates and β-CD-MA, the destroy of the hydrogen bonding interaction between templates and the polymeric network, and shrinkage of polymer network (Fig. 1b).

The interactions between the template and the functional monomers are of great importance for enhancing the adsorption capability and selectivity properties of the imprinted polymers. The optimal ratios between β-CD or MAA with template were studied by UV–Vis spectroscopy, respectively. Furthermore, we need to note that in the range of measured wavelength, MAA and β-CD didn't appear any characteristic peaks [38–40]. Firstly, in order to explore the interaction of MAA with BPA, we kept the concentration of BPA at predetermined concentration while varied the concentration of MAA. The absorption of BPA placed at 225 nm was shifted increasingly to longer wavelengths and even disappeared along with an increase in MAA concentration, while the peak of BPA at 278 nm didn't shift, which was consistent well with the results reported by Xie et al. [38]. The changes in absorption wavelength of BPA suggested that the hydrogen bonding interaction between hydroxyl of aromatic guest molecules and carboxyl group of MAA happened. Moreover, the adsorption spectrum at 225 nm turned to unchanged while MAA/BPA ratio reached to greater than 3:1, as shown in Fig. 2a. The above results implied that the optimal stoichiometry between the MAA and BPA was 3:1. Fig. 2b showed UV–vis absorption spectra of BPA to different molar ratio of β-CD. Except for the significant red-shift in adsorption peak of BPA at 225 nm, there was also

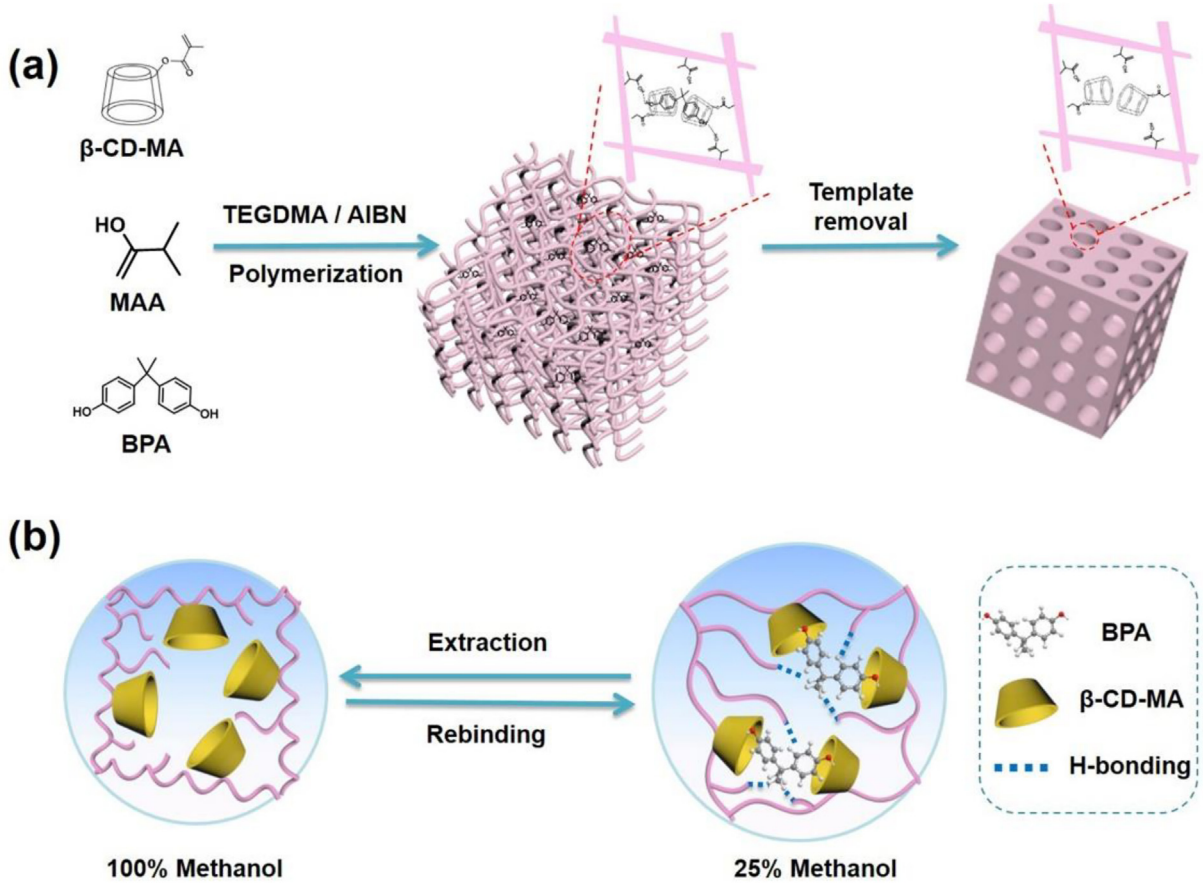

Fig. 1. Schematic illustrations for the preparation of S-MIPs (a) and possible recognition mechanism of S-MIPs for templates (b).

a slight red-shift at 278 nm, which can be attributed to the successful formation of inclusion complexes between BPA and β-CD. Takashi's group [41,42] has also reported the similar phenomena. In short, the stable template-monomer complex formed when the ratio of β-CD and BPA is 2:1. As demonstrated in Fig. 2c, the interaction of MAA/β-CD/BPA was further measured to obtain the optimal ratios (3:2:1). Furthermore, the corresponding MIPs were prepared to verify the adsorption capacity. As shown in Fig. 2d, the highest bound was obtained while the MAA/β-CD/BPA ratio was arranged as 3:2:1.

3.2. Characterization

Fig. 3a presents the FT-IR spectra of β-CD and β-CD-MA. The infrared spectra of both β-CD and β-CD-MA exhibited peaks of 3383 cm^{-1} (O—H), 2930 cm^{-1} (C—H), 1155 cm^{-1} (C—O) and 1027 cm^{-1} (C—O—C), implying that the synthesized β-CD-MA did not change the skeleton structure of β-CD. Moreover, compared with β-CD, the infrared spectra of β-CD-MA showed the stretching vibration peaks of C═O (1720 cm^{-1}) and C═C (1637 cm^{-1}), demonstrating that the acryloyl group has been successfully transferred to β-CD by substitution reaction. Fig. 3b indicates the FT-IR spectra of S-MIPs and S-NIPs. As for S-MIPs and S-NIPs, they both presented the characteristic peaks of β-CD seen at 2930 cm^{-1} (C—H) and 1027 cm^{-1} (C—O—C). The absorption bands at 1720 cm^{-1} in S-MIPs could belong to the C═O stretching vibration of carboxyl of MAA. And the adsorption bands at 1265 cm^{-1} and 1165 cm^{-1} in S-MIPs could be attributed to the C—O symmetric and asymmetric stretching vibration of ester of TEGDMA, respectively. The above results suggested the successful formation of imprinted layer. Comparing the characteristic peaks of S-MIPs with that of S-NIPs, there was no obvious difference indicating that the complete removal of templates.

The morphologies and microstructures of the constructed S-MIPs and S-NIPs were clearly visualized by SEM. As presented in Fig. 4a, the SEM micrographs of S-MIPs showed that amount of irregular micropores were embedded in the polymer network, probably due to the fact that templates were able to influence the morphologies of polymers [43]. We believe that multi-porous structure of S-MIPs would contribute to higher surface area thus enhancing adsorption capability. However, the morphologies of S-NIPs showed densely surface, indicating that there were no porous holes in S-NIPs (Fig. 4b). In addition, nitrogen adsorption and desorption experiments of S-MIPs and S-NIPs were carried out. The nitrogen adsorption–desorption isotherms of S-MIPs exhibited IV-type curves (Fig. S1). The Brunauer-Emmett-Teller (BET) surface area, average pore size and total pore volume of S-MIPs are 3.02 m^2/g, 278.50 nm and 0.019 cm^3/g, respectively. According to the nitrogen adsorption–desorption results of S-NIPs, there was no nitrogen adsorption for S-NIPs. The results were consistent with the SEM images, demonstrating the densely compact structure of S-NIPs.

The thermo-stability of S-MIPs was demonstrated by TGA. Fig. 5a showed the TGA curves of S-MIPs and S-NIPs in the temperature range from 25 to 800 °C. The weight losses of S-MIPs can be divided into two steps: step 1, the removal of physically and chemically adsorbed water between 100 and 200 °C, respectively; step 2, the removal of the organic content in the imprinting layer when the temperature climbs above 200 °C. Therefore, S-MIPs and S-NIPs could possess the excellent thermo-stability below 200 °C.

When the S-MIPs were dispersed in methanol-water solution with different composition, the average size of imprinting materials changed significantly (Fig. 4a, c, d). Obviously, the higher content of methanol in circumstance medium, accompanying with the reduction of water content, would lead to the shrinkage of imprinting material. It is presumed that due to the presence of cross-linker TEGDMA, S-MIPs

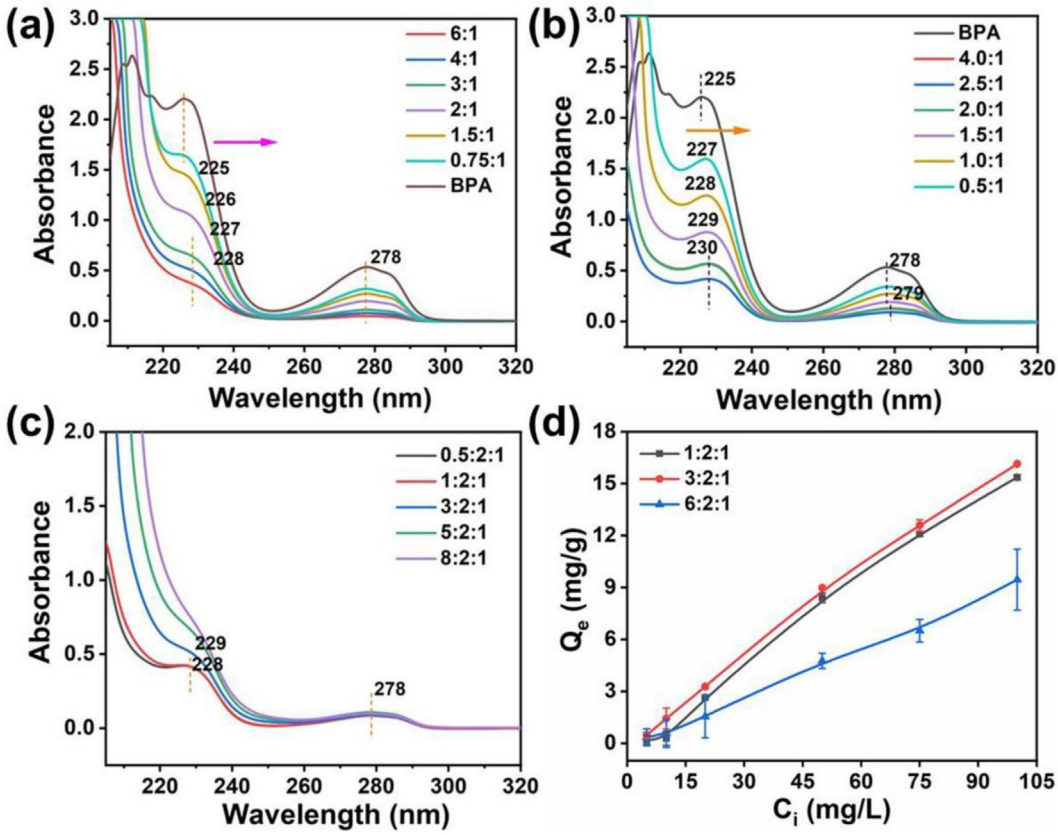

Fig. 2. UV–vis absorption spectra of BPA to different molar ratio of MAA (a); BPA to different molar ratio of β-CD (b); β-CD/BPA (ratio fixed at 2/1) to different molar ratio of MAA (c); binding amount of BPA on different MIPs (d).

displayed dynamic size in different methanol-water mixtures. The similar results published by Kim et al were consistent well with this work [38]. When dispersed in 50% methanol aqueous solution, cross-linker embedded in materials displayed less flexible structure compared to that in 25% methanol aqueous solution causing the shrinkage of S-MIPs. By comparison, imprinting materials showed the much smaller size in 100% methanol. Interestingly, the de-swelled imprinting materials can be swelled by changing the solvent back to 25% methanol aqueous solution. The phenomena above may presumably impact recognition property of S-MIPs: the imprinted binding sites could match well with the target molecules in 25% methanol aqueous solution, whereas changing the solvent composition (i.e., from 25% methanol aqueous solution to 100% methanol), the polymeric network shrinks, with consequent deformation of the binding sites and loss of recognition.

3.3. Binding properties of the S-MIPs

3.3.1. Adsorption equilibrium of S-MIPs

To demonstrate the rebinding features of the S-MIPs, static adsorption equilibrium experiments were conducted. At the onset of the experiments, the adsorption capacity of S-MIPs and S-NIPs increased rapidly together with the increase of initial concentration in Fig. 6a. However, the adsorption rate tended to slow down at a certain concentration of BPA due to gradual saturation of existing recognition sites. Compared with S-NIPs, the S-MIPs possessed the higher adsorption capacity, which meant that the imprinted sites were successfully formed in S-MIPs. Furthermore, the Langmuir and Freundlich models

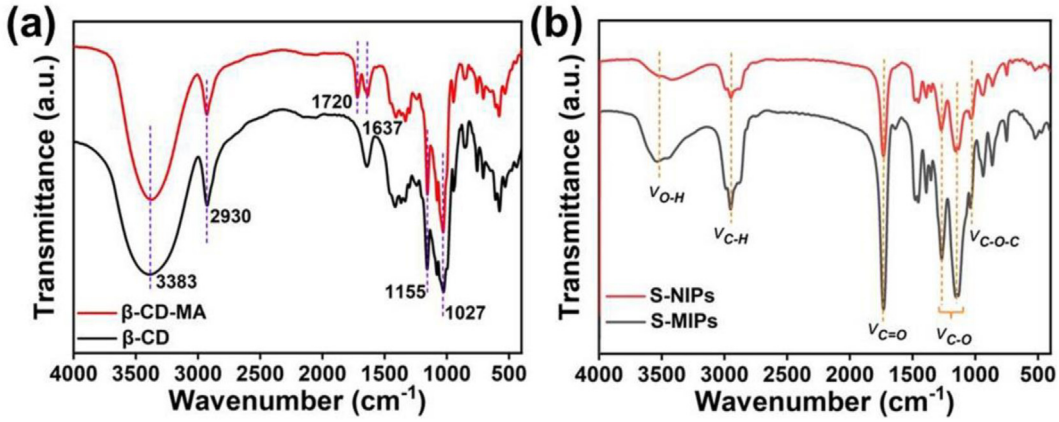

Fig. 3. FT-IR spectra of β-CD and β-CD-MA (a); S-MIPs and S-NIPs (b).

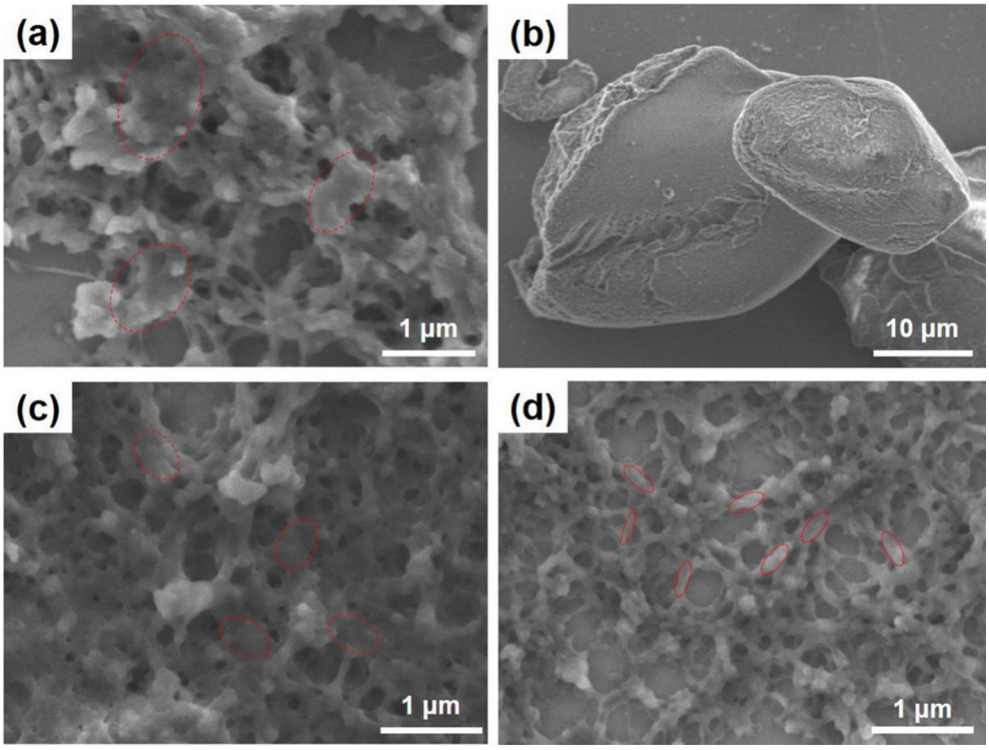

Fig. 4. SEM images of S-MIPs in 25% methanol aqueous solution (a); S-NIPs in 25% methanol aqueous solution (b); S-MIPs in 50% methanol aqueous solution (c); S-MIPs in 100% MeOH (d).

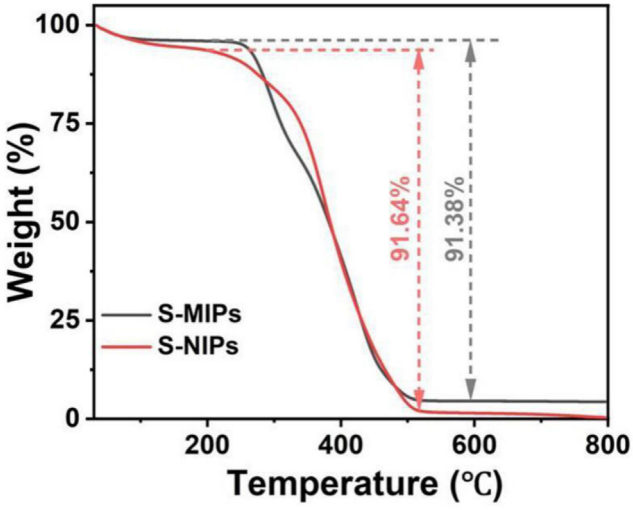

Fig. 5. TGA curves of S-MIPs and S-NIPs in the range of 25–800 °C.

were utilized for assessing the isotherm binding process and the corresponding equations were expressed as Eq. (S-1) and Eq. (S-2), respectively. The fitting curves have illustrated in Fig. 6b, c. The curves simulated by the Langmuir model indicated relatively larger correlation coefficients (0.999), consistent well with the adsorption curves (Table 1). In general, the Langmuir model demonstrates that active sites onto surface of absorbents are homogeneous, causing the monolayer binding. The maximum adsorption capacity for BPA onto S-MIPs was reached to 21.36 mg/g, whereas the capacity of S-NIPs was 13.16 mg/g, which suggested that S-MIPs consisted of amount of binding sites with excellent imprinting effect. The results were well line with SEM images. In the same circumstance media, S-MIPs possessed plenty of micropores with more binding sites and did bind to the BPA with high affinity. However, S-NIPs showed densely surface without molecule transfer channels, which was not benefit for recognition thus causing the low adsorption capacity.

3.3.2. Adsorption kinetics of S-MIPs

The extended binding kinetics of BPA onto absorbents were carried out. As shown in Fig. 6d, the adsorption amounts of BPA increased quickly in the beginning 30 min and gradually slow down till equilibrium. The dynamic curves of S-NIPs appeared a similar tendency while displaying a lower adsorption capacity. The discrepancy in adsorption capacity would be explained by the following factors: in the preparation process of S-MIPs, functional monomer β-CD-MA hosted the templates to form the pre-assembly complex, at the same time, the joint of MAA strengthened the imprinted interaction. After the polymerization and further removal of templates, S-MIPs possessed a lot of recognition sites, which were matched well with the template molecules in size, shape and chemical functionality. However, functional monomers in S-NIPs were kept in a state of disordered, thus causing the unmatched sites for templates. On the other hand, S-MIPs showed multi pores providing a lot of accessible routes to binding sites, while S-NIPs exhibited non-porous surface structure causing the unaccessible channels for templates. So, it would take a longer time for S-NIPs to reach adsorption equilibrium. Therefore, S-MIPs displayed a high binding rate for BPA, while S-NIPs presented a lower binding rate. The pseudo-first-order and pseudo-second-order models were further applied for fitting analysis according to the Eq. (S-3) and Eq. (S-4). As shown in Fig. 6f, the dynamic data can be well described by pseudo-second-order kinetics model (Table 2).

3.3.3. Adsorption selectivity

To get more detailed information about the binding characteristics, the binding selectivity of S-MIPs was also estimated by comparing the binding amounts between template and its structural analogues, demonstrated in Fig. 7. The adsorption capacities of S-MIPs for BPA, DPA and RF were measured in 25% methanol aqueous solution as 8.97, 0.60, 0.82 mg/g, respectively. And the corresponding selectivity factors were

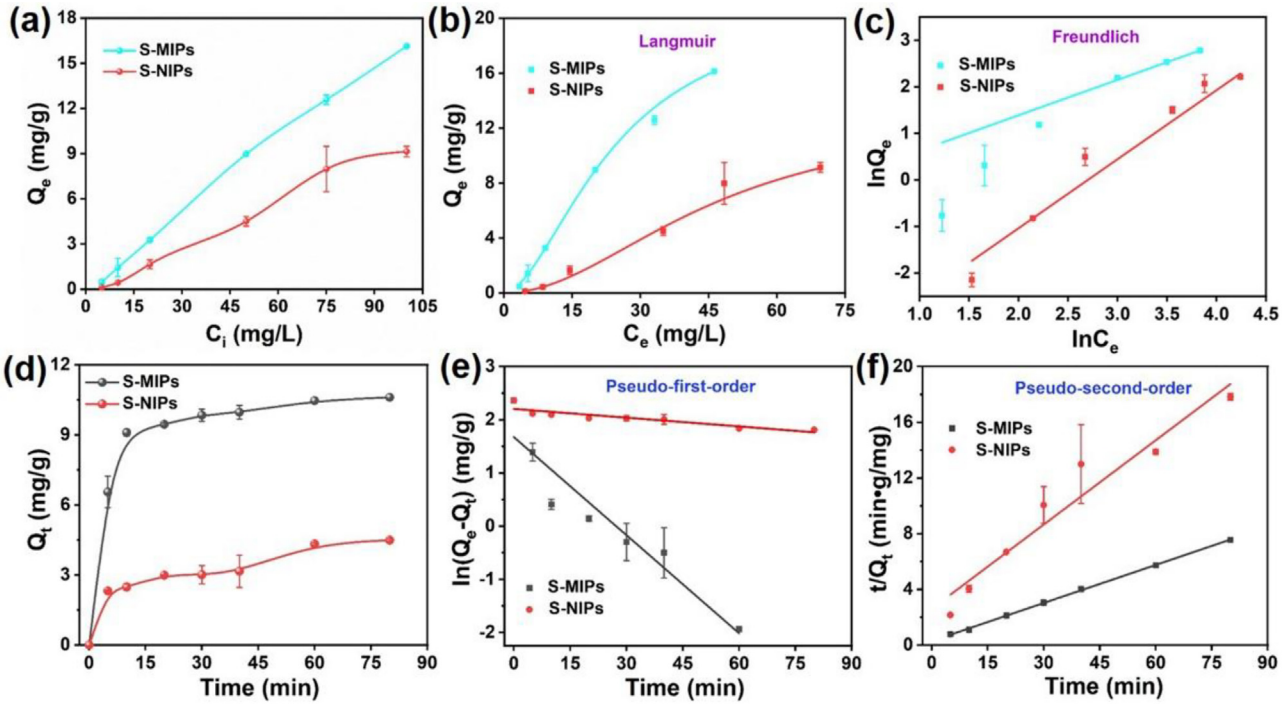

Fig. 6. Adsorption isotherms (a): Langmuir model (b); Freundlich model (c). And adsorption kinetics (d): Pseudo-first-order model (e); Pseudo-second-order model (f) of BPA binding onto S-MIPs and S-NIPs.

Table 1
Isotherm parameters for BPA binding by S-MIPs and S-NIPs from the two isotherm models.

Adsorbents	Langmuir			Freundlich		
	q_m (mg/g)	K (L/mg)	R^2	lnK_f (mg/g)	$1/n$	R^2
S-MIPs	21.364	0.00381	0.999	−0.133	0.761	0.976
S-NIPs	13.160	4.818	0.995	−4.00	1.483	0.995

Table 2
Kinetic parameters for BPA binding by S-MIPs and S-NIPs from the two kinetic models.

Adsorbents	Pseudo-first-order kinetics			Pseudo-second-order kinetics		
	lnq_e (mg/g)	k_1 (min^{-1})	R^2	q_e (mg/g)	k_2(g mg^{-1} min^{-1})	R^2
S-MIPs	1.675	0.0615	0.905	10.982	0.0289	0.999
S-NIPs	2.204	0.00549	0.808	4.96	0.0156	0.941

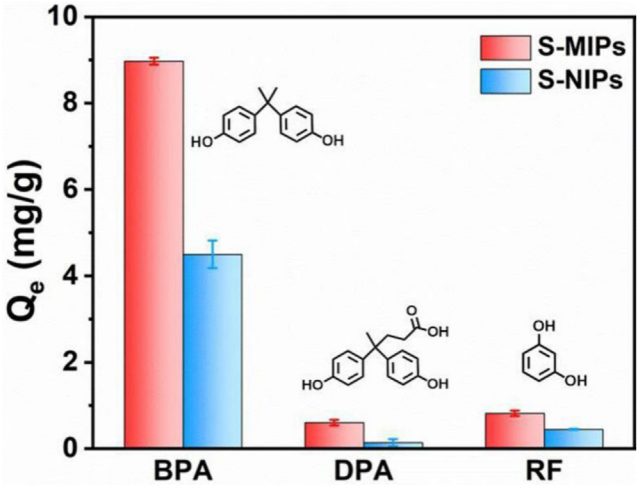

Fig. 7. Binding selectivity of S-MIPs and S-NIPs for BPA and its structural analogs in 25% methanol aqueous solution.

14.95, 10.94, respectively. The abovementioned results directly indicated that S-MIPs had better binding affinity toward BPA than its structural analogues, whose shapes or functional groups could not perfectly match with the imprinting cavities or recognition sites in S-MIPs. The binding capacities of S-NIPs for all three analytes were all lower than those of S-MIPs. However, the S-NIPs possessed higher affinity for BPA than other two analogues. The interaction between three structural analogues and S-NIPs is mainly the host–guest interaction between analogues and β-CD, as well as hydrogen bonding interaction between analogues and polymeric networks. Compared to that of BPA, the long alkyl chain structure of DPA increases its cyclotron diameter, making it difficult to match with cavity of β-CD well [44]. And RF possesses higher hydrophilicity, which is not conducive to binding with hydrophobic cavity of β-CD. So it is difficult for DPA and RF to interact with β-CD by host–guest interaction. In addition, because of the absence of template in the polymerization process, the S-NIPs possessed a compact structure without pores (confirmed by nitrogen adsorption and desorption experiments and SEM images). So the hydrogen bonding interaction between analogs (DPA and RF) and the polymeric network is very small, resulting in the low adsorption capacity. By contrast, although the hydrogen bonding between BPA and the polymeric network of S-NIPs is also small, BPA can form a good host–guest inclusion with β-CD. So the adsorption capacity of S-NIPs for BPA is higher than that of DPA and RF. All the above results suggested that S-MIPs exhibited higher selectivity and affinity toward BPA.

3.4. Solvent-regulated binding behavior of BPA

Fig. 8a showed the changes of adsorption capacity of S-MIPs and S-NIPs along with variation of water content in methanol aqueous solution. When immersed in 100% methanol, S-MIPs couldn't adsorb any templates, that is, the adsorption capacity of imprinting materials is

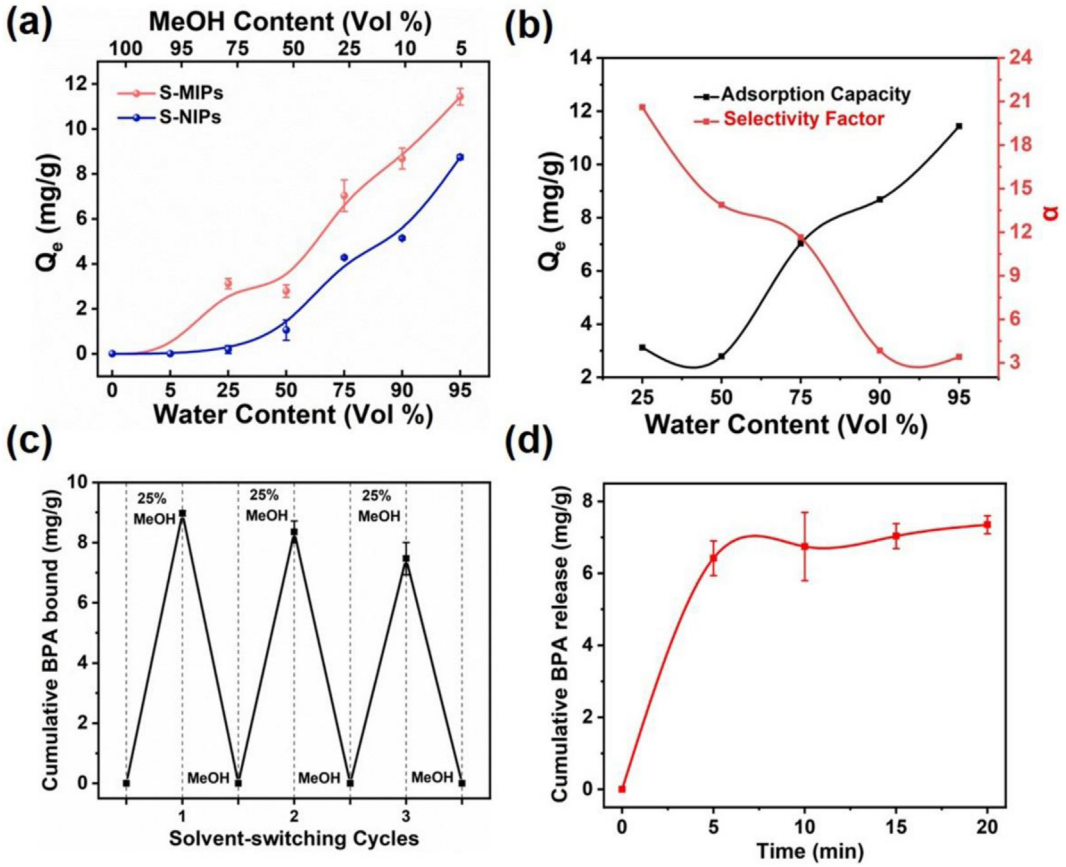

Fig. 8. (a) BPA binding curves of S-MIPs and S-NIPs upon the increase of water content; (b) the changes of adsorption capacity and selectivity factor of S-MIPs upon the increase of water content; (c) solvent-regulated binding behavior of BPA by the S-MIPs; (d) BPA release curve in 100% methanol.

close to zero. With the water content in solution increased, the adsorption capacity gradually developed. We further investigated the changes of the adsorption selectivity of S-MIPs with different solvent composition (Fig. 8b). We should note that BPA is water insoluble. DPA with similar structure and the same solubility was introduced as control. With the water content in solution increased, the adsorption selectivity gradually decreased, which was exactly contrary to the change trend of adsorption capacity. For adsorbents applied to sample pretreatment, the selectivity factors and adsorption capacity of adsorbents should be taken into consideration simultaneously. So we chose 25% methanol aqueous solution to carry out subsequent experiments.

The solvent-responsive template binding properties were carried out under the repetitive solvent-switching conditions. Fig. 8c demonstrated the amount of bound BPA changes of S-MIPs in different media. Obviously, the affinity of S-MIPs for BPA has distinctly changed when the solvent composition switched from 25% methanol aqueous solution to 100% methanol. When the solution changes from 25% methanol aqueous solution to 100% methanol, about 97.8% of the adsorbed BPA molecules in S-MIPs were released. Interestingly, 93.1% of the released templates were rebound into S-MIPs again after exchanging the solution to 25% methanol aqueous solution for another 60 min, which was well consistent with the swelling property of S-MIPs through changing the solvent composition back to 25% methanol aqueous solution. Rebinding phenomenon of S-MIPs verified its solvent-induced reversibility. Even after several cycles, the release and uptake of BPA in quantity was similar to that of the previous cycle, which further proved S-MIPs not only possessed the excellent solvent-responsiveness, but also showed the good repeatability. We further monitored the templates release process in methanol (Fig. 8b). The data demonstrated that the templates adsorbed in S-MIPs released completely into methanol within only 10 min, which satisfied the demands of rapid analysis in the practical application.

Based on the above experimental results, the possible mechanism for solvent-regulated adsorption of BPA was discussed. The adsorption mechanism of S-MIPs to BPA is mainly attributed to the host–guest interaction and hydrogen bonding interaction between BPA and imprinting sites, as well as high matching of three-dimensional size with imprinted cavity. In 25% methanol aqueous solution, recognition sites in S-MIPs matched well with the templates in size, shape and functional group, displaying high affinity to templates. However, in 100% methanol, the host–guest interaction between BPA and β-CD was destroyed (Fig. S2), meanwhile, changes in the three-dimensional network structure of S-MIPs (Fig. 4d) caused the destruction of hydrogen bonding interaction between BPA and polymeric network, and the deformation of imprinted cavity, which cannot match the size of BPA. The BPA adsorbed in S-MIPs could be almost completely released in 100% methanol. Thereby, the newly imprinting materials possessed excellent solvent reversibility. Such a facile controlled release and uptake by solvent regulation will give the imprinted materials more practical application.

3.5. Analysis of BPA in human urine

3.5.1. Optimization of extraction conditions

The optimization of extraction conditions was carried out [44–47] by extracting 5 mL BPA aqueous solution (2000 μg/L). Several parameters, such as extraction time, amount of S-MIPs and desorption conditions were firstly investigated to acquire the desired experiment effect. As seen in Figure S3, the optimal conditions acquired: 70 mg of S-MIPs was added and reached equilibrium within 30 min, and then 4 mL methanol was used to elute for four times (4 × 1 mL) assisted by ultrasound. Under the above optimal conditions, the satisfactory

Table 3
Recoveries of BPA obtained from human urine samples.

Sample	Added (μg/L)	Found (μg/L)	Recovery (%)	RSD (n = 3, %)
Human urine	0	ND	–	–
	40	30.9	77.3	7.2
	400	346.7	86.6	2.8
	800	701.7	87.8	3.1

recoveries of BPA were obtained, offering a foundation for the subsequent detection of BPA in human urine.

3.5.2. Human urine analysis

The prepared S-MIPs were used as the materials of solid phase extraction to selectively extract BPA in human urine samples under the above optimal experiments conditions, followed by HPLC-DAD determination. The linear range obtained for the determination of BPA was 20–1000 μg/L with a correlation coefficient of 0.999. And the limit of detection (LOD) for BPA was 1.7 μg/L based on the analyte concentration producing signal/noise ratio of 3:1. A comparison between this method and previously reported BPA extraction methods was shown in Table S1. No BPA at detectable levels were found in the urine obtained from a healthy volunteer. Then the recovery study was carried out by spiking the urine samples with BPA at three spiked levels of 40, 400 and 800 μg/L, respectively. Table 3 clearly indicated that the recoveries at three spiked levels of BPA were from 77.3% to 87.8%, demonstrating the potential capability of S-MIPs for separating BPA from urine samples. The utilization of solvent-regulated intelligent elution method by S-MIPs provides a simple strategy for BPA analysis in real biological samples. On the one hand, an efficient elution induced by 100% methanol not only gets rid of the addition of a conventional acid which is necessary in conventional MIPs elution process, but also perfectly fits with the subsequent chromatographic analysis conditions. On the other hand, protein pre-deposition is not required for samples preparation, which significantly simplified samples pre-treatment process. The above results successfully suggested that the S-MIPs can be directly utilized to separate and enrich BPA with high selectivity and enrichment ability in practical samples.

4. Conclusions

In this work, we firstly developed a universal method to prepare the smart molecularly imprinting material with solvent-tunable adsorption performances, namely S-MIPs. Instead of designing the complicated functionality-complementary functional monomer with stimuli-responsiveness, utilization of solvent-responsive cross-linker can easily impart imprinting materials with excellent switchable adsorption characters. This strategy takes the advantages of simple and convenient synthesis with great versatility. The binding experiments demonstrated that the introduction of solvent-responsiveness of cross-linker triethylene glycol dimethacrylate endowed the S-MIPs with superior solvent-regulation binding character. The S-MIPs can easily bind template molecules in 25% methanol aqueous solution with high affinity and excellent selectivity while release the templates in 100% methanol. Moreover, the S-MIPs were directly and successfully utilized to extract BPA from human urine samples with excellent enrichment capability and satisfactory recovery. We strongly believe that exploiting and employing the smart cross-linker will be one of the future development directions of intelligent molecularly imprinting materials preparation.

Declaration of Competing Interest

The authors declare that they have no known competing financial interests or personal relationships that could have appeared to influence the work reported in this paper.

Acknowledgments

This work was supported by Development Program of the Ministry of Science and Technology of Jilin Province, China (No. 20180201011GX) and Basic Frontier Program of Jilin University (No. 45119031C129).

Appendix A. Supplementary data

Supplementary data to this article can be found online at https://doi.org/10.1016/j.cej.2020.126608.

References

[1] T. Zhou, L. Ding, G. Che, W. Jiang, L. Sang, Recent advances and trends of molecularly imprinted polymers for specific recognition in aqueous matrix: preparation and application in sample pretreatment, TrAC-Trend. Anal. Chem. 114 (2019) 11–28.
[2] F. Barahona, B. Albero, J.L. Tadeo, A. Martín-Esteban, Molecularly imprinted polymer-hollow fiber microextraction of hydrophilic fluoroquinolone antibiotics in environmental waters and urine samples, J. Chromatogr. A 1587 (2019) 42–49.
[3] R. Garcia, M.D.R.G. da Silva, M.J. Cabrita, "On-off" switchable tool for food sample preparation: merging molecularly imprinting technology with stimuli-responsive blocks. Current status, challenges and highlighted applications, Talanta 176 (2018) 479–484.
[4] A. Ostovan, M. Ghaedi, M. Arabi, Q. Yang, J. Li, L. Chen, Hydrophilic multitemplate molecularly imprinted biopolymers based on a green synthesis strategy for determination of B-family vitamins, ACS Appl. Mater. Interfaces 10 (2018) 4140–4150.
[5] J. Luan, K.K. Liu, S. Tadepalli, Q. Jiang, J.J. Morrissey, E.D. Kharasch, S. Singamaneni, PEGylated artificial antibodies: plasmonic biosensors with improved selectivity, ACS Appl. Mater. Interfaces 8 (2016) 23509–23516.
[6] Z. Altintas, M. Gittens, A. Guerreiro, K.A. Thompson, J. Walker, S. Piletsky, I.E. Tothill, Detection of waterborne viruses using high affinity molecularly imprinted polymers, Anal. Chem. 87 (2015) 6801–6807.
[7] J. Matsui, K. Akamatsu, S. Nishiguchi, D. Miyoshi, H. Nawafune, K. Tamaki, N. Sugimoto, Composite of Au nanoparticles and molecularly imprinted polymer as a sensing material, Anal. Chem. 76 (2004) 1310–1315.
[8] J. Chen, S. Lei, Y. Xie, M. Wang, J. Yang, X. Ge, Fabrication of high-performance magnetic lysozyme-imprinted microsphere and its NIR-responsive controlled release property, ACS Appl. Mater. Interfaces 7 (2015) 28606–28615.
[9] H.Y. Wang, P.P. Cao, Z.Y. He, X.W. He, W.Y. Li, Y.H. Li, Y.K. Zhang, Targeted imaging and targeted therapy of breast cancer cells via fluorescent double template-imprinted polymer coated silicon nanoparticles by an epitope approach, Nanoscale 11 (2019) 17018–17030.
[10] X.F. Zheng, Q. Lian, H. Yang, X. Wang, Surface molecularly imprinted polymer of chitosan grafted poly(methyl methacrylate) for 5-fluorouracil and controlled release, Sci. Rep. 6 (2016) 21409.
[11] Z. Zhang, X. Zhang, B. Liu, J. Liu, Molecular imprinting on inorganic nanozymes for hundred-fold enzyme specificity, J Am. Chem. Soc. 139 (2017) 5412–5419.
[12] Z. Zhang, Y. Li, X. Zhang, J. Liu, Molecularly imprinted nanozymes with faster catalytic activity and better specificity, Nanoscale 11 (2019) 4854–4863.
[13] J.J. BelBruno, Molecularly imprinted polymers, Chem. Rev. 119 (2019) 94–119.
[14] S. Farooq, J. Nie, Y. Cheng, Z. Yan, J. Li, S.A.S. Bacha, A. Mushtaq, H. Zhang, Molecularly imprinted polymers' application in pesticide residue detection, Analyst 143 (2018) 3971–3989.
[15] A. Speltini, A. Scalabrini, F. Maraschi, M. Sturini, A. Profumo, Newest applications of molecularly imprinted polymers for extraction of contaminants from environmental and food matrices: a review, Anal. Chim. Acta 974 (2017) 1–26.
[16] L. Chen, X. Wang, W. Lu, X. Wu, J. Li, Molecular imprinting: perspectives and applications, Chem. Soc. Rev. 45 (2016) 2137–2211.
[17] J.-P. Fan, J.-X. Yu, X.-M. Yang, X.-H. Zhang, T.-T. Yuan, H.-L. Peng, Preparation, characterization, and application of multiple stimuli-responsive rattle-type magnetic hollow molecular imprinted poly (ionic liquids) nanospheres (Fe3O4@void@PILMIP) for specific recognition of protein, Chem. Eng. J. 337 (2018) 722–732.
[18] X. Xie, Q. Hu, R. Ke, X. Zhen, Y. Bu, S. Wang, Facile preparation of photonic and magnetic dual responsive protein imprinted nanomaterial for specific recognition of bovine hemoglobin, Chem. Eng. J. 371 (2019) 130–137.
[19] Y. Kanekiyo, R. Naganawa, H. Tao, pH-responsive molecularly imprinted polymers, Angew. Chem. 42 (2003) 3014–3016.
[20] W. Li, K. Dong, J. Ren, X. Qu, A beta-lactamase-imprinted responsive hydrogel for the treatment of antibiotic-resistant bacteria, Angew. Chem. 55 (2016) 8049–8053.
[21] H. Liu, Y. Li, K. Sun, J. Fan, P. Zhang, J. Meng, S. Wang, L. Jiang, Dual-responsive surfaces modified with phenylboronic acid-containing polymer brush to reversibly capture and release cancer cells, J Am. Chem. Soc. 135 (2013) 7603–7609.
[22] W.F. Zhao, B.H. Fang, N. Li, S.Q. Nie, Q. Wei, C.S. Zhao, Fabrication of pH-responsive molecularly imprinted polyethersulfone particles for bisphenol-A uptake, J. Appl. Poly. Sci. 113 (2009) 916–921.
[23] T. Renkecz, G. Mistlberger, M. Pawlak, V. Horvath, E. Bakker, Molecularly imprinted polymer microspheres containing photoswitchable spiropyran-based binding sites, ACS Appl. Mater. Interfaces 5 (2013) 8537–8545.

[24] Y. Liu, G. Zhong, Z. Liu, M. Meng, F. Liu, L. Ni, Facile synthesis of novel photo-responsive mesoporous molecularly imprinted polymers for photo-regulated selective separation of bisphenol A, Chem. Eng. J. 296 (2016) 437–446.
[25] L. Fang, S. Chen, Y. Zhang, H. Zhang, Azobenzene-containing molecularly imprinted polymer microspheres with photoresponsive template binding properties, J. Mater. Chem. 21 (2011) 2320–2329.
[26] L. Pan, G. Zhai, X. Yang, H. Yu, C. Cheng, Thermosensitive microgels-decorated magnetic graphene oxides for specific recognition and adsorption of Pb(II) from aqueous solution, ACS Omega 4 (2019) 3933–3945.
[27] S. Li, Y. Ge, S.A. Piletsky, A.P.F. Turner, A zipper-like on/off-switchable molecularly imprinted polymer, Adv. Func. Mater. 21 (2011) 3344–3349.
[28] T. Shiraki, A. Dawn, Y. Tsuchiya, S. Shinkai, Thermo- and solvent-responsive polymer complex created from supramolecular complexation between a helix-forming polysaccharide and a cationic polythiophene, J Am. Chem. Soc. 132 (2010) 13928–13935.
[29] X. Wu, X. Wang, W. Lu, X. Wang, J. Li, H. You, H. Xiong, L. Chen, Water-compatible temperature and magnetic dual-responsive molecularly imprinted polymers for recognition and extraction of bisphenol A, J. Chromatogr. A 1435 (2016) 30–38.
[30] S. Xu, H. Lu, X. Zheng, L. Chen, Stimuli-responsive molecularly imprinted polymers: versatile functional materials, J. Mater. Chem. C 1 (2013) 4406.
[31] W. Chen, Y. Ma, J. Pan, Z. Meng, G. Pan, B. Sellergren, Molecularly imprinted polymers with stimuli-responsive affinity: progress and perspectives, Polymers 7 (2015) 1689–1715.
[32] Y. Ge, B. Butler, F. Mirza, S. Habib-Ullah, D. Fei, Smart molecularly imprinted polymers: recent developments and applications, Macromol. Rapid Comm. 34 (2013) 903–915.
[33] J. Aburto, S. Le Borgne, Selective adsorption of dibenzothiophene sulfone by an imprinted and stimuli-responsive chitosan hydrogel, Macromolecules 37 (2004) 2938–2943.
[34] V.P. Joshi, R.N. Karmalkar, M.G. Kulkarni, R.A. Mashelkar, Effect of solvents on selectivity in separation using molecularly imprinted adsorbents: separation of phenol and bisphenol A, Ind. Eng. Chem. Res. 38 (1999) 4417–4423.
[35] M. Bertolla, L. Cenci, A. Anesi, E. Ambrosi, F. Tagliaro, L. Vanzetti, G. Guella, A.M. Bossi, Solvent-Responsive molecularly imprinted nanogels for targeted protein analysis in MALDI-TOF mass spectrometry, ACS Appl. Mater. Interfaces 9 (2017) 6908–6915.
[36] L.P. Zhang, X.L. Wang, Q.Q. Pang, Y.P. Huang, L. Tang, M. Chen, Z.S. Liu, Solvent-responsive floating liquid crystalline-molecularly imprinted polymers for gastro-retentive controlled drug release system, Int. J. Pharmaceut. 532 (2017) 365–373.
[37] E. Kim, J. Lee, D. Kim, K.E. Lee, S.S. Han, N. Lim, J. Kang, C.G. Park, K. Kim, Solvent-responsive polymer nanocapsules with controlled permeability: encapsulation and release of a fluorescent dye by swelling and deswelling, Chem. Comm. 28 (2009) 1472–1474.
[38] K. Yongfeng, D. Wuping, L. Yan, K. Junxia, X. Jing, Molecularly imprinted polymers of allyl-β-cyclodextrin and methacrylic acid for the solid-phase extraction of phthalate, Carbohyd. Polym. 88 (2012) 459–464.
[39] Y. Liu, Y. Liu, Z. Liu, F. Du, G. Qin, G. Li, X. Hu, Z. Xu, Z. Cai, Supramolecularly imprinted polymeric solid phase microextraction coatings for synergetic recognition nitrophenols and bisphenol A, J. Hazard. Mater. 368 (2019) 358–364.
[40] S. Wang, B. Wang, H. Si, J. Shan, X. Yang, Preparation of magnetic molecularly imprinted polymer beads and their recognition for baicalein, RSC Adv. 5 (2015) 8028–8036.
[41] A. Kawamura, T. Kiguchi, T. Nishihata, T. Uragami, T. Miyata, Target molecule-responsive hydrogels designed via molecular imprinting using bisphenol A as a template, Chem. Comm. 50 (2014) 11101–11103.
[42] K. Matsumoto, A. Kawamura, T. Miyata, Conformationally regulated molecular binding and release of molecularly imprinted polypeptide hydrogels that undergo helix–coil transition, Macromolecules 50 (2017) 2136–2144.
[43] S. Ansari, S. Masoum, Ultrasound-assisted dispersive solid-phase microextraction of capecitabine by multi-stimuli responsive molecularly imprinted polymer modified with chitosan nanoparticles followed by HPLC analysis, Microchim. Acta 187 (2020) 366.
[44] Z. Lin, R. Wang, H. Gong, H. Jiang, Synthesis of β-cyclodextrin crossing resins and its adsorption properties for diphenolic acid, Fine Chem. 35 (2018) 1719.
[45] S. Liu, C. Lai, B. Li, C. Zhang, M. Zhang, D. Huang, L. Qin, H. Yi, X. Liu, F. Huang, X. Zhou, L. Chen, Role of radical and non-radical pathway in activating persulfate for degradation of p-nitrophenol by sulfur-doped ordered mesoporous carbon, Chem. Eng. J. 384 (2020) 123304.
[46] X. Zhou, Z. Zeng, G. Zeng, C. Lai, R. Xiao, S. Liu, D. Huang, L. Qin, X. Liu, B. Li, H. Yi, Y. Fu, L. Li, Z. Wang, Persulfate activation by swine bone char-derived hierarchical porous carbon: Multiple mechanism system for organic pollutant degradation in aqueous media, Chem. Eng. J. 383 (2020) 123091.
[47] X. Zhou, C. Lai, D. Huang, G. Zeng, L. Chen, L. Qin, P. Xu, M. Cheng, C. Huang, C. Zhang, C. Zhou, Preparation of water-compatible molecularly imprinted thiol-functionalized activated titanium dioxide: selective adsorption and efficient photodegradation of 2, 4-dinitrophenol in aqueous solution, J. Hazard. Mater. 346 (2018) 113–123.